Theoretical and experimental study on mechanical properties and flexural strength of fly ash-geopolymer concrete

CrossMark

Khoa Tan Nguyen [a], Namshik Ahn [a], Tuan Anh Le [b], Kihak Lee [a,*]

[a] Sejong University, Department of Architectural Engineering, Seoul 143-747, South Korea
[b] Vietnam National University of Ho Chi Minh City, Faculty of Civil Engineering, Viet Nam

HIGHLIGHTS

- Young's modulus of geopolymer concrete were affected by its microstructure.
- Stress–strain relation of geopolymer concrete is same as Portland cement concrete.
- The tensile strength of geopolymer concrete is greater than that of normal concrete.
- The actual geopolymer beam is stiffer than the theoretical analysis model.
- The deflections at mid-spans determined from FEM are matched well with the test data.

ARTICLE INFO

ABSTRACT

In this paper, evaluation of the mechanical properties of heat-cured low-calcium fly-ash geopolymer concrete and the behavior of geopolymer concrete beams are reported in detail. The mechanical properties are evaluated using the modulus elasticity, Poisson's ratio, stress–strain relation, and indirect tensile strength. Behavior of the geopolymer beam is determined using a flexural test with four-point bending, elastic theory, and a finite element model (FEM). The measured modulus elasticity values of geopolymer concrete are lower than those calculated using current standards for normal concrete. The Poisson's ratio is from 0.16 to 0.21, which is similar to the values of conventional concrete. The stress–strain relation in compression matches well with the formulation designed for Portland cement concrete. The indirect tensile strength is a fraction of the compressive strength but it is higher than the calculated value using an expression designed for normal concrete. The deflections at mid-span, and the crack patterns of the geopolymer concrete beam determined from FEM, are better matched with the experimental results than with the elastic theory results.

1. Introduction

Global warming is caused by the emission of excessive greenhouse gases into the atmosphere by human activities, and carbon dioxide (CO_2) is responsible for about 65% of global warming. The global cement industry contributes around 6% of all CO_2 emissions because the production of one ton of Portland cement releases approximately one ton of CO_2 into the atmosphere [1,2]. Some researchers have stated that CO_2 emission could increase by 50% compared with the present scope [3,4]. Therefore, the impact of cement production on the environment issues a significant challenge to concrete industries in the future. As a result, it is necessary to find a new concrete material to replace traditional

Portland cement concrete, which is environmentally stressful, yet provides an effective building material [5]. To this end, geopolymer concrete is a breakthrough development providing an essential alternative to conventional cement, using novel, low-cost, environmentally friendly materials [6]. Geopolymers are inorganic aluminosilicates produced by alkali activation solutions and source materials. Thus, geopolymer concrete is created using activated industrial waste materials such as fly ash in the presence of sodium hydroxide and sodium silicate solutions. It also has involves a geopolymerization process that is widely different from the hydration process of Portland cement [7].

Almost all research on geopolymers has determined that this new binder has great potential as an alternative to ordinary Portland cement (OPC). Geopolymers have received considerable attention because geopolymer materials may result in environmental benefits such as reduction in consumption of natural resources

---

Nomenclature

Abbreviation	
FEM	Finite element model
CO_2	carbon dioxide
OPC	ordinary Portland cement
RGPC	reinforced geopolymer concrete
CA	coarse aggregate
FA	fine aggregate
LVDT	Liner Variable Differential Transducer
l	length of specimen in splitting tensile strength
d	diameter of specimen in splitting tensile strength
a_o, b_o, L_o	Dimensions in the undeformed configuration
θ_A, θ_C	Bending angles at supports and at load application points in four bending
δ_C	Displacement of the load application points in a four-point bending test
I	Moment of inertia with respect to the middle plane
$Q = P/2$	Applied load at each node in four-point bending
b, h	Width and thickness of the specimen
E	Young's modulus
η_A, η_C	Terms related to support span and load span reduction in a four-point bending test
f_{ct}	splitting tensile strength
M_a	maximum moment in member at stage of deflection is computed
I_{cr}	moment of inertia of cracked, transformed section
I_g	moment of inertia of gross concrete section-neglect reinforcement
y_t	distance from neutral axis to tension face
f_c', f_{cm}	the specified 28-day compressive strength of concrete
f_r	the tensile strength of concrete
ρ	density of concrete
v	Poisson's ratio
σ	Stress (MPa)
ε	Strain

---

and decrease in the net production of CO_2. Geopolymer concrete is an innovative binder material that could totally replace Portland cement. Geopolymer concrete utilizes solid industrial aluminosillicate-based waste materials such as fly ash, rice husk ash, and silica fume to produce an environmentally friendly and low-cost alternative to Portland cement.

Until recently, the understanding of structural geopolymer concrete was extremely limited. Some of the research carried out has been comparative study of experimental and analytical aspects of geopolymer concrete members. Broke et al. [8] reported that the behavior of geopolymer concrete beam–column joints was similar to that of members of Portland cement concrete. Uma [9] performed a flexural response of reinforced geopolymer concrete (RGPC) beams. The results from both ANSYS modeling and experimental data were compared, and revealed that the deflection obtained was low due to meshing of elements in the model. They also concluded that the comparative result gave a 20% difference between the experimental and ANSYS results. The results from the research by Curtin University on fly-ash-based geopolymer concrete is described in research report GC3 [10]. They concluded that the behavior of geopolymer concrete beams is similar to those of reinforced Portland cement concrete, and good correlation between the test and calculated values was found.

In order to have a deeper understanding of the characteristics and behavior of structural geopolymer concrete, this study was intended to evaluate the following properties of fly ash-geopolymer concrete: stress–strain relation in compression, Young's modulus, Poisson's ratio, and splitting tensile strength. The behavior of geopolymer concrete beams subjected to a four-point bending test was also investigated using experimental tests, theoretical-analysis-based elastic theory, and simulation software (ABAQUS).

2. Materials and methods

2.1. Materials

Low-calcium fly ash known as 'Class F' based on ASTM, with specific gravity 2500 kg/m³, was used in this study. This fly ash came from a power station. Enlarged particles of it are shown in an SEM image (Fig. 1a) and dry bulk in Fig. 1b. Details of the chemical composition of the fly ash are presented in Table 1.

Solutions of sodium silicates and sodium hydroxide were mixed to create the combination called alkaline liquid. The components of the sodium silicate solution were Na_2O and SiO_2 (approximately 36–38% by mass). Coarse aggregates (20 mm and 10 mm, CA) and fine aggregates (FA) were used. The ratio between coarse aggregates and fine aggregates was 40% (20 mm), 30% (10 mm) and 30% (fine aggregate). The specific gravity of the coarse aggregates was 2700 kg/m³ and 2650 kg/m³ for the fine aggregates.

Details of the mix proportions used in this study are shown in Table 2. For all mix proportions, the concentration of sodium hydroxide solution was 8 M. Water glass and sodium hydroxide were mixed in the ratios 1, 2, and 2.5 by mass. Besides this, the ratios between alkali solutions (including water glass and sodium hydroxide) and fly ash were 0.4, 0.5 and 0.6. In Table 2, the name of the mixtures is GPCx, which stands for geopolymer concrete number x (where x = 1, 2, or 3). The ratio of alkali liquid to fly ash was 0.6 for GPC1, 0.5 for GPC2, and 0.4 for GPC3. The ratio of sodium silicate to sodium hydroxide was the same for all mix proportions and equaled 2.5. In the results and discussion section, the name of group data is GPCx – ab, (where ab is the curing temperature, ab = 60, 90, or 120 °C).

2.2. Specimen preparation and curing condition

Geopolymer concrete includes coarse aggregate, fine aggregate, alkaline liquid, fly ash and water. The two aggregates and the fly ash are quantified before mixing. Alkaline liquid is a combination of water glass and sodium hydroxide solution. To make sodium liquid solution, sodium hydroxide solids were mixed with the water. Then, the sodium hydroxide solution was mixed with the water glass. This liquid was prepared one day before mixing day. According to Davidovits [5], the alkaline liquid should be mixed first, and it would make the polymerization easier.

The manufacturing process shown in Fig. 2, includes three steps:

– Step 1: All solids are mixed together about three minutes after quantifying by mixer machine or by hand. The amount used is determined by the amount required for the number of specimens needed.
– Step 2: The alkali liquid, which is prepared one day before, is poured over the solids. Then they are mixed together for about four minutes.
– Step 3: The fresh geopolymer concrete is cast and compacted into the molds. Right after finishing this step, the specimens are sent to an oven and cured. Time and temperature depend on the needs of the tests used.

2.3. Test methods

In this research, the test program was separated into two parts: one about the mechanical properties of the fly-ash-based geopolymer concrete, and one about the behavior of a geopolymer beam subjected to a four-point bending test. In Table 3, information about the testing procedure is summarized. The details of the tests are presented below.

2.3.1. Compressive strength

The standard ASTM C39/C 39M-99 [11], covers determination of the compressive strength of cylindrical concrete specimens, such as cylinders. This test method is used to apply a compressive axial load to molded cylinders at a rate from 0.15 to 0.35 MPa/s, until failure occurs. The compressive strength of geopolymer concrete specimens is determined by dividing the maximum load attained during the test, by the cross-sectional area of the concrete specimen. Concrete cylinders of 150 mm diameter and 300 mm height were cured in the oven and tested after aging for 7 d.
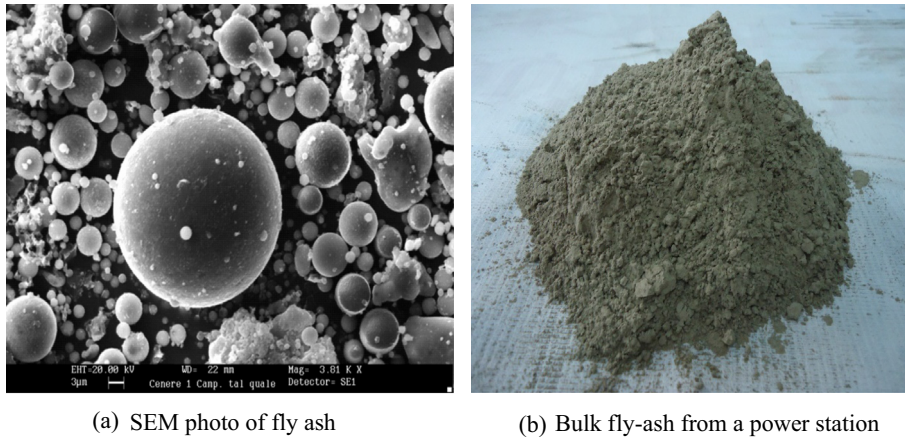
(a) SEM photo of fly ash

(b) Bulk fly-ash from a power station

Fig. 1. Class-F fly ash.

Table 1
Chemical composition of fly ash.

Oxide	SiO$_2$	Al$_2$O$_3$	Fe$_2$O$_3$	CaO	K$_2$O & Na$_2$O	MgO	SO$_3$	LOI
(%)	51.7	31.9	3.48	1.21	1.02	0.81	0.25	9.63

Table 2
Mixture proportions of experimental concrete.

Mix	CA (kg/m^3)	FA (kg/m^3)	Fly ash (kg/m^3)	Sodium silicate solution (kg/m^3)	Sodium hydroxide solution (kg/m^3)
GPC1	1079	593	418	179	72
GPC2	1113	612	431	154	62
GPC3	1149	632	445	127	51
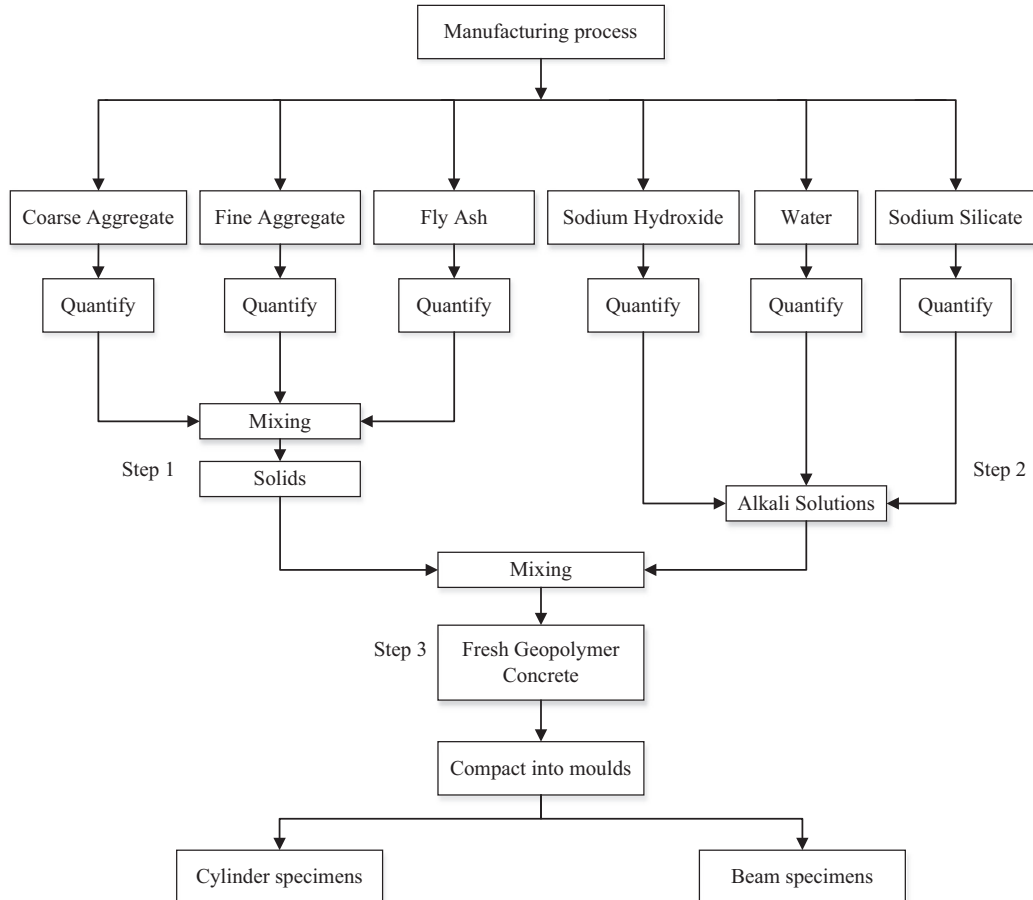
Fig. 2. Geopolymer concrete manufacturing process.

Table 3
Mechanical testing for fly-ash geopolymer concrete.

Name of test	Reference	Test way	Details
Compressive strength	ASTM C39/ C39M-99		Test specimens: cylinder 150 mm × 300 mm Test age: 7 d Rate of loading: 0.15–0.35 MPa/s
Stress–strain relation	ASTM C469		Test specimens: cylinder 150 mm × 300 mm Test age: 7 d Rate of loading: 241 ± 34 kPa/without interruption of loading Specimens shall be tested within 1 h after removal from curing or storage room.
Indirect tensile strength	ASTM C496		Test specimens: cylinder 150 mm × 300 mm Test age: 7 d Rate of loading: a constant rate within the range 689–1380 kPa/min splitting tensile stress until failure of specimen

2.3.2. Stress–strain behavior

Another standard, ASTM C469 [12] was used to obtain the modulus of elasticity (Young's) and Poisson's ratio of molded concrete cylinders under longitudinal compressive stress. This test method also provides a stress–strain relation. Three Linear Variable Differential Transducer (LVDTs) were used and fixed at the mid-height of a cylinder. Two LVDTs (left and right sides) were used to measure the lateral deformation, and a centrally placed LVDT was used to measure longitudinal deformation. Note that the load must be applied continuously and without shock. The rate of loading was within the range 241 ± 34 kPa/s. The specimens (150 × 300 mm) were cured at 60, 90, and 120 °C for 10 h. These specimens were tested after curing for 7 d.

Young's modulus and Poisson's ratio were obtained as follows:

$$E = \frac{(S_1 - S_2)}{\varepsilon_2 - 0.000050} \tag{1}$$

where

E: modulus of elasticity, MPa
S_2: stress corresponding to 40% of ultimate load, MPa
S_1: stress corresponding to longitudinal strain, ε_1, of 50 millionths, MPa
ε_2: longitudinal strain produced by stress S_2

$$v = \frac{(\varepsilon_{t2} - \varepsilon_{t1})}{(\varepsilon_2 - 0.000050)} \tag{2}$$

where

v: Poisson's ratio
ε_{t2}: transverse strain at mid height of the specimen produced by stress S_2
ε_{t1}: transverse strain at mid height of specimen produced by stress S_1

2.3.3. Indirect tensile strength

ASTM C496 [13] covers determination of the splitting tensile strength of molded cylindrical concrete specimens. This test method is used to apply a diametral compressive force along the length of a cylindrical specimen at a rate from 689 to 1380 kPa/min, until failure occurs. This loading causes tensile stresses on the plane containing the applied load, and relatively high compressive stresses in the area immediately around the applied load. As above, 150 × 300 mm specimens were cured at 60, 90, and 120 °C for 4, 6, 8, and 10 h, and then tested after 7 d.

Splitting tensile strength of fly ash geopolymer concrete was determined as follows:

$$f_{ct} = \frac{2P}{\pi l d} \tag{3}$$

where

f_{ct}: splitting tensile strength (MPa)
P: maximum applied load indicated by the testing machine (MN)
l: length (mm)
d: diameter (mm)

2.3.4. Flexural performance of fly ash-geopolymer concrete (using beam with four-point bending)

The dimensions of the beam specimens were 100 (b) × 200 (h) × 2000 mm (L). The geopolymer beams were cast in steel molds. The details of the beams are shown in Fig. 3, and the schematic of the four-point bending test is presented in Fig. 4. In this test, three LVDTs were used to measure the mid-span deflection of geopolymer concrete beam. Freshly prepared geopolymer concrete was poured into molds and compacted in three layers of the same thickness. All the beams were oven cured
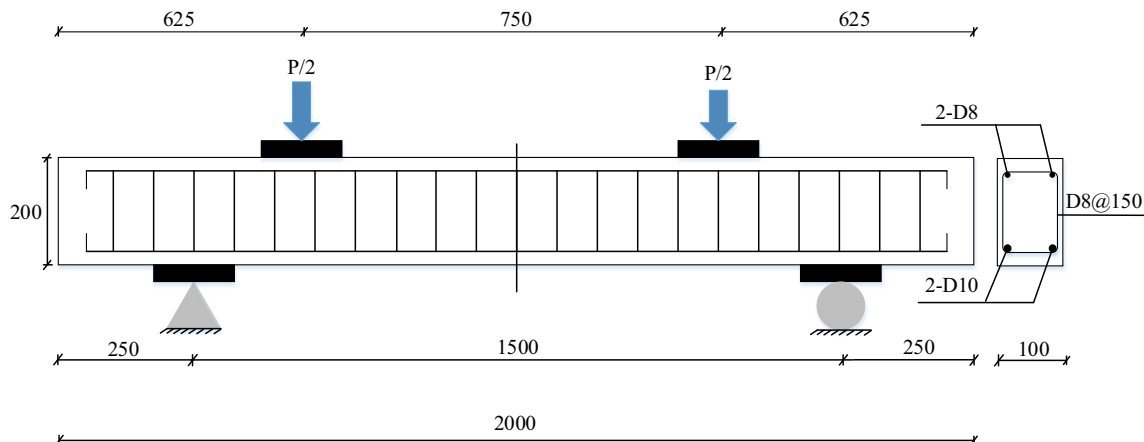

Fig. 3. Details of the experimental geopolymer concrete beam.
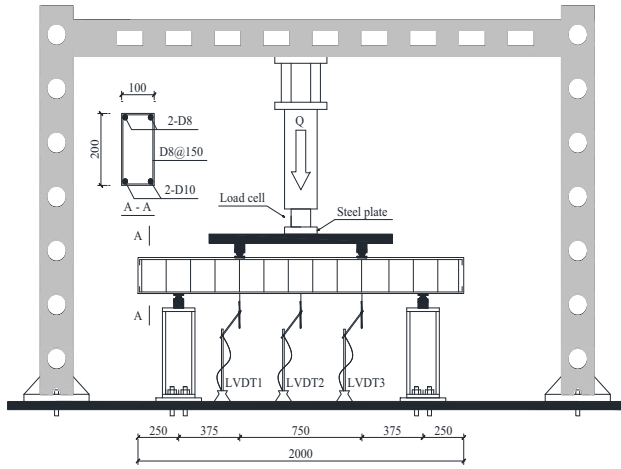
Fig. 4. Schematic of the four-point bending test.

under the same curing conditions as for the cylindrical specimens. In order to reduce local stress at the supports and load rollers, four steel plates were added to the beam specimen. The size of a plate was $100\,(b) \times 6\,(h) \times 100$ mm (L). In these tests, the mixtures GPC1, GPC2, and GPC3 would be cured at 60 °C for 4 h.

3. Theoretically analysis

In order to reduce the errors at the supports and load application points in the case of four-point bending, Mujika [14] proposed a new formula to calculate the deflection of the four-point bending test.

The system in Fig. 5 was used as the basic system for calculation of displacement and angles. For the four-point bending test, displacement and angles can be obtained using the principle of superposition. The results needed for the basic system can be obtained, for instance, using the conjugate beam method without considering shear effects.
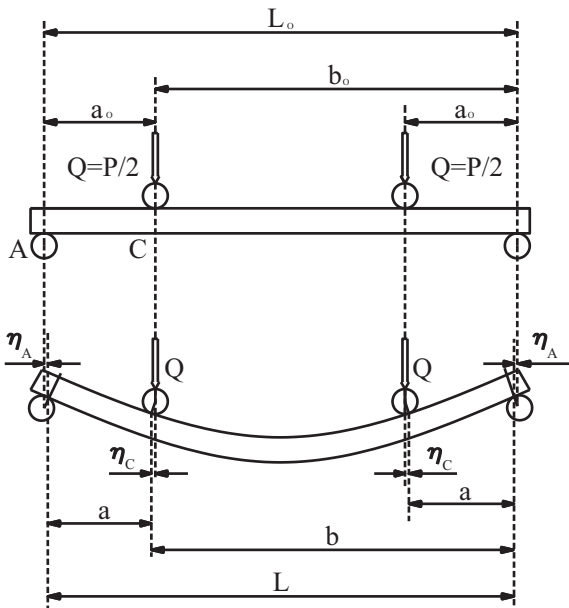

Fig. 5. Un-deformed (top) and deformed (bottom) conditions for the four-point bending test [14].

$$L = L_o - 2\eta_A$$
$$a = a_o - \eta_A - \eta_C = a_o - \eta_1$$
$$\eta_1 = \eta_A + \eta_C \tag{4}$$
$$b = b_o - \eta_A + \eta_C = b_o - \eta_2$$
$$\eta_2 = \eta_A - \eta_C$$

The error terms at supports and at load applications points are:

$$\eta_A = \theta_A R_A$$
$$\eta_C = \theta_C R_C \tag{5}$$

The angle at supports θ_A and the angle at load application point θ_C are:

$$\theta_A = \frac{Qa_o b_o}{2EI}$$
$$\theta_C = \frac{Qa_o(b_o - a_o)}{2EI} \tag{6}$$

The displacement at center of the beam is:

$$\delta_{center} = \frac{Q}{EI}\left(-\frac{1}{8}aL^2 + \frac{1}{6}a^3\right) \tag{7}$$

Replacing a, b, L from Eq. (4) results in

$$\delta_{center} = \frac{Q(a_o - \eta_1)}{EI}\left[-\frac{1}{8}(L_o - 2\eta_A)^2 + \frac{1}{6}(a_o - \eta_1)^2\right] \tag{8}$$

Neglecting small terms in the parentheses of Eq. (8) results in

$$\delta_{center} = \frac{Q(a_o - \eta_1)}{EI}\left(\frac{1}{2}L_o\eta_A - \frac{1}{3}a_o\eta_1 - \frac{1}{8}L_o^2 + \frac{1}{6}a_o^2\right) \tag{9}$$

Eq. (9) is valid for any load span in a four-point bending. In the experimental part of the present work, quarter point loading was used, being $a_o = L_o/4$. Replacing these values and taking into account that $Q = P/2$ results in

$$\delta_{center} = \frac{PL_o}{24EI}\left[\frac{1}{4}L_o - (\eta_A + \eta_C)\right][-L_o + 2\eta_A - 4\eta_C] \tag{10}$$

In order to calculate η_A and η_C replacing the mentioned values of a_o and b_o in Eq. (6), the angles at points A and C are

$$\theta_A = \frac{3PL_o^2}{16EI}$$
$$\theta_C = \frac{PL_o^2}{16EI} \tag{11}$$

From Eqs. (5) and (11) the terms η_A and η_C are

$$\eta_A = \frac{3PL_o^2}{16EI}R_A$$
$$\eta_C = \frac{PL_o^2}{16EI}R_C \tag{12}$$

From Eqs. (10) and (12) the displacement at center point is

$$\delta_{\text{center}} = \frac{PL_o}{24EI}\left[\frac{1}{4}L_o - \left(\frac{3PL_o^2}{16EI}R_A + \frac{PL_o^2}{16EI}R_C\right)\right]\left[-L_o + \frac{3PL_o^2}{8EI}R_A - \frac{PL_o^2}{4EI}R_C\right]$$

(13)

From now on, the displacement at the center point of a geopolymer concrete beam are calculated by Eq. (13).

According to ACI 318 [15], for moments at or below the cracking moment, the moment of inertia is that of the un-cracked transformed section. At moments larger than the cracking moment, behavior is complex and the effective moment of inertia (I_e) of the beam would be used:

$$I_e = \left(\frac{M_{cr}}{M_a}\right)^3 I_g + \left[1 - \left(\frac{M_{cr}}{M_a}\right)^3\right]I_{cr} \leqslant I_g$$

(14)

where

$$M_{cr} = \frac{f_r I_g}{y_t} \quad \text{and} \quad f_r = 7.5\sqrt{f_c'}$$

M_a: maximum moment in member at stage of deflection is computed
I_{cr}: moment of inertia of cracked, transformed section
I_g: moment of inertia of gross concrete section-neglect reinforcement
y_t: distance from neutral axis to tension face
f_c': the specified 28-day compressive strength of concrete
f_r: the tensile strength of concrete

4. Finite element model

In this part, a 3D FE model of a geopolymer concrete beam, reinforcement bars, stirrups, and steel plates was built employing ABAQUS/CAE structural analysis modeling tool, to simulate a four-point bending test. The experimental test was conducted using the beam model shown in Figs. 3 and 4. Figs. 6 and 7 show the model of the beam and deflection of the beam in the ABAQUS model.
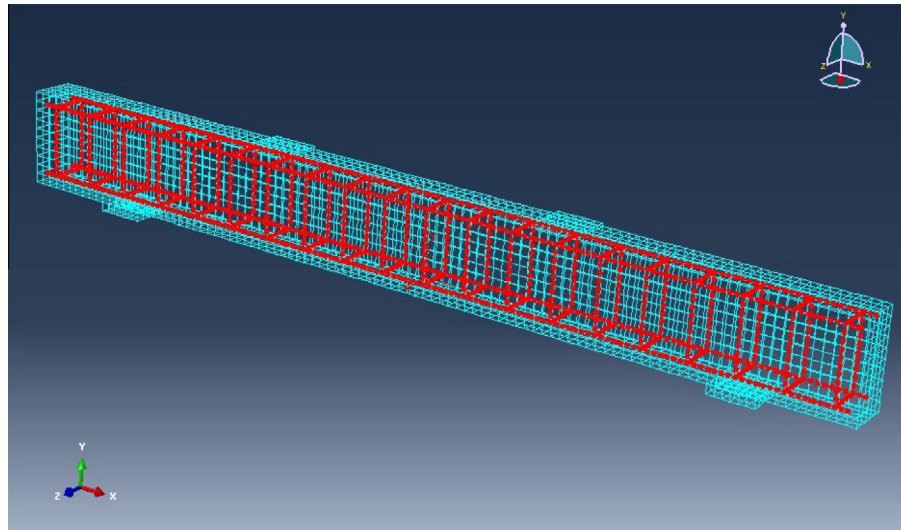

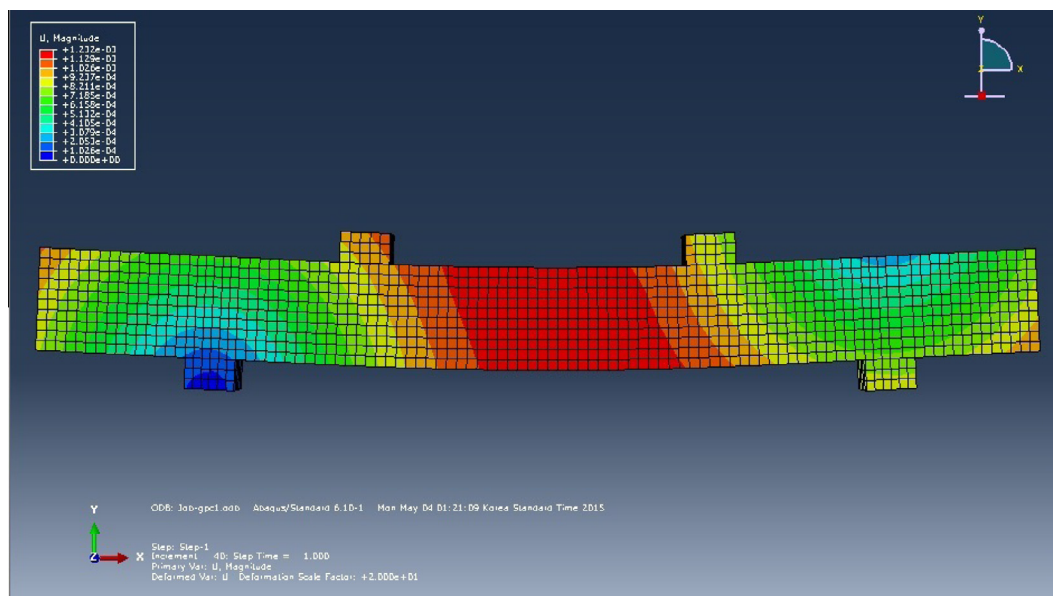Fig. 6. Finite element model in ABAQUS.

Fig. 7. Deflection of beam indicated by ABAQUS model.

Table 4
Parameters for experimental concrete used in this research.

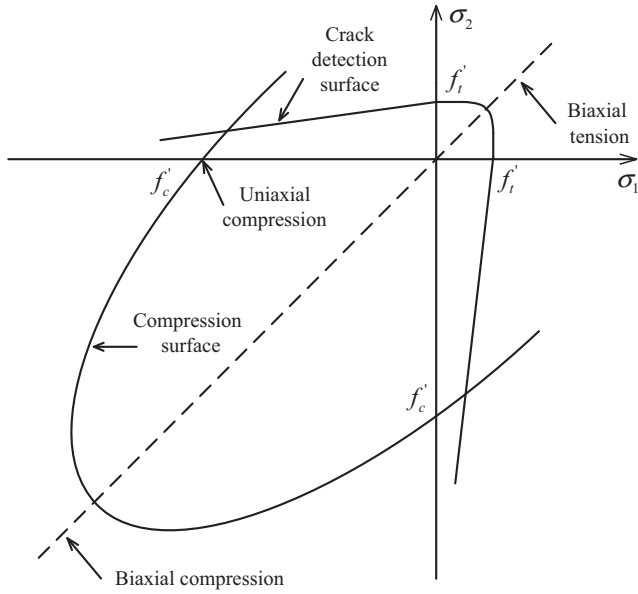| Mix	f'_c (MPa)	E_c (GPa)	v	f_{ct} (MPa)	ρ (kg/m³)
GPC1	30	20.13	0.22	3.46	2400
GPC2	25	18.84	0.22	3.21	2400
GPC3	20	17.41	0.22	2.93	2400

Fig. 8. Concrete failure surface from in plane stress [16].

Fig. 9. Uniaxial compression test of geopolymer concrete.

Fig. 10. Tension stiffening model.

4.1. Concrete

The properties of the fly-ash geopolymer concrete, including uniaxial compressive strength of f'_c, Young's modulus, Poisson's ratio, tensile strength f_{ct} and the density, are given in Table 4. These data were determined from experimental tests.

The concrete failure strength is different under multiaxial combinations and those occurring under uniaxial status (Fig. 8). It seems that the load path does not affect the maximum strength of concrete under multiaxial loading. In ABAQUS, the failure surface of the concrete was modeled using a type of Mohr–Coulomb type compression surface together with a crack detection surface. The concrete response was modeled using the elastic–plastic theory, in which the principal stress components of the concrete are mainly compressive, and the concrete was modeled with an isotropic hardening rule and an associated flow (Fig. 8).

The orientation of the crack was stored once the crack is defined as occurring in tension. A certain parameter was needed to guide the yield surface expansion when plastic deformation occurred. The stress–strain curves for geopolymer concrete are presented in Fig. 9.

When concrete cracking occurs, the crack behavior is represented and used to define a damage plasticity model. After cracking, concrete still has some tensile strength in the direction normal to the crack, which is termed tension stiffening. In this research, the tension stiffening phenomenon was modeled (Fig. 10).

The concrete damaged plasticity model (CDP) was used for defining the concrete material behavior in the inelastic range. Lee and Han [17], developed this model. Tensile cracking and compressive crushing are the main failure mechanisms of the concrete in th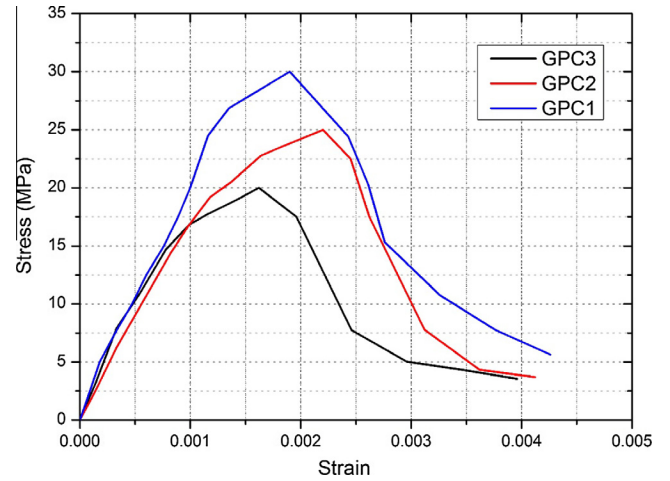e concrete damaged plasticity model. The program computes the concrete compressive stress–strain curve based on the input of stress versus inelastic strain. The concrete behavior under axial tension is assumed to be linear until formation of the initial cracking at the peak stress (known as the failure stress). Post failure stress is defined in the program in terms of stress versus cracking strain. This behavior allows for the effect of interaction between the concrete and reinforcement rebar by introducing tension stiffening to the softening side of the curve.

4.2. Steel bar, stirrup and steel plate and FE model

Steel bars have approximately linear elastic behavior when the steel stiffness introduced by the Young's modulus is constant at low strain. At higher strain values, they begin to have nonlinear, inelastic behavior, which is referred to as plasticity. On the other hand, their behavior is the same as an elastic–plastic material. The rebar and concrete-cracking behavior were considered independently [18]. The properties of the steel bars used in the reinforced beam are given in Table 5.
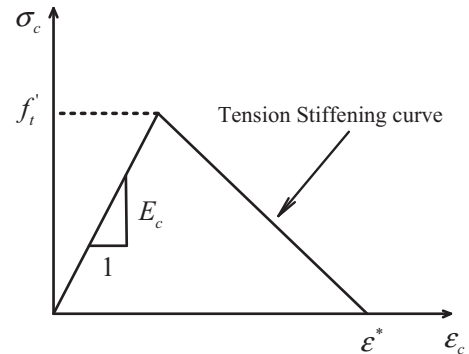
Table 5
Properties of reinforcing steel bar used in experimental concrete.

Properties	Value
Density	7800 kg/m³
Young's modulus	200 GPa
Yielding stress	410 MPa
Poisson's ratio	0.3

Table 6
Young's modulus and Poisson ratio from tests.

Mix	Curing temperature (°C)	Young's modulus E_c (GPa)	Poisson ratio v
GPC1	60	25.10	0.18
	90	25.40	0.19
	120	24.20	0.19
GPC2	60	21.90	0.18
	90	25.50	0.16
	120	24.90	0.18
GPC3	60	22.80	0.19
	90	22.60	0.21
	120	28.00	0.19

These values in Table 5 were also used for the stirrups and steel plates. Full bond contact between the steel reinforcement and concrete was assumed. The embedded element option was used for connecting the reinforcement element to the concrete element. The steel reinforcement was used as the embedded element and the concrete was designated as the host element.

In order to determine accurate results from the FE model, all the elements in the model were assigned the same mesh size to ensure that each different materials share the same node. The type of mesh selected in the model was structured.

5. Results and discussions

5.1. Modulus of elasticity and Poisson's ratio

Mixtures GPC1, GPC2, and GPC3 with curing conditions: 60, 90, and 120 °C for 10 h, were used to measure the modulus of elasticity and Poisson's ratio. The modulus of elasticity or Young's modulus, was calculated as the secant modulus measured at the stress value equal to 40% of the average compressive strength of concrete cylinders, according to ASTM C469. The test data are shown in Table 6.

In Table 6, the Poisson's ratio range of fly ash-based geopolymer concrete is from 0.16 to 0.21, while Poisson's ratio of normal concrete lies generally in the range from 0.15 to 0.22 [19]. The value of 0.15 is for high-strength concrete and 0.22 for low-strength concrete. This range is the same as for the values measured for the geopolymer concrete in this research.

The value of Young's modulus of fly-ash-based geopolymer concrete is about 22.8–28 GPa. By comparison, the modulus of elasticity of normal concrete is from 34.16 GPa to 38.33 GPa. It seems that the Young's modulus of geopolymer concrete is lower than conventional concrete. According to Duxon [20], Young's modulus of geopolymer concrete is affected by microstructure based on speciation of the alkali silicate activating solutions. This is one difference between geopolymer and normal concrete; in the latter, Young's modulus depends on the properties of the aggregate [19].
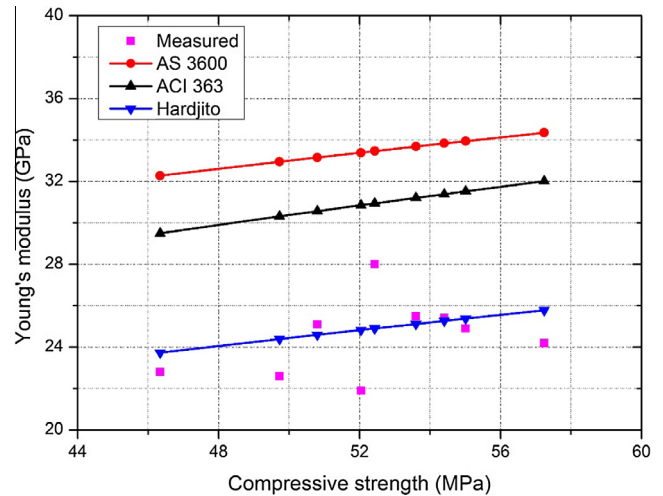

Fig. 11. Relationship between Young's modulus and compressive strength of geopolymer concrete.

For ordinary Portland cement concrete, the America Concrete Institute, ACI 363 [21] recommends the following expressions to determine the value of the modulus of elasticity:

$$E_C = 3320\sqrt{f'_c} + 6900 \text{ (MPa)} \tag{15}$$

The Australia standard (AS) 3600 [22] recommended the following expression to calculate the modulus of elasticity within an error of ±20%:

$$E_C = \rho^{1.5} \times \left(0.024\sqrt{f_{cm}} + 0.12\right) \text{ (MPa)} \tag{16}$$

Also, Hardjito [23] proposed the following expression to calculate the modulus of elasticity:

$$E_C = 2707\sqrt{f_{cm}} + 5300 \text{ (MPa)} \tag{17}$$

where

f'_c, f_{cm} is the mean compressive strength in MPa
ρ is the unit-weight of geopolymer concrete in kg/m^3

The average unit-weight of geopolymer concrete was 2350 kg/m^3. Table 7 and Fig. 11 show a comparison between the measured value of the modulus of elasticity in this study and the value calculated by Eqs. (15)–(17). Noted that only Eq. (17) is designed for use with geopolymer concrete.

In Fig. 11, the value of Young's modulus of geopolymer concrete is smaller than OPC. Eqs. (15) and (16) are used to calculate the value of the modulus of elasticity of normal concrete when compressive strength is given. The difference between the measured and calculated values using Eqs. (15) and (16) was 30–40%. Thus,

Table 7
Comparison between modulus elasticity values measured and those calculated using AS3600, ACI 363, and Hardjito.

Mix	Compressive strength (MPa)	E_c measured (GPa)	E_c (AS 3600) (GPa)	E_c (ACI 363) (GPa)	E_c (Hardjito) (GPa)
GPC1–60	50.80	25.1	33.16	30.56	24.59
GPC1–90	54.40	25.4	33.84	31.39	25.27
GPC1–120	57.24	24.2	34.36	32.02	25.78
GPC2–60	52.04	21.9	33.39	30.85	24.83
GPC2–90	53.60	25.5	33.69	31.31	25.12
GPC2–120	55.01	24.9	33.95	31.52	25.38
GPC3–60	46.34	22.8	32.28	29.5	23.73
GPC3–90	49.73	22.6	32.95	30.31	24.39
GPC3–120	52.43	28	33.47	30.94	24.9

Table 8
Stress–strain of experimental geopolymer concrete.

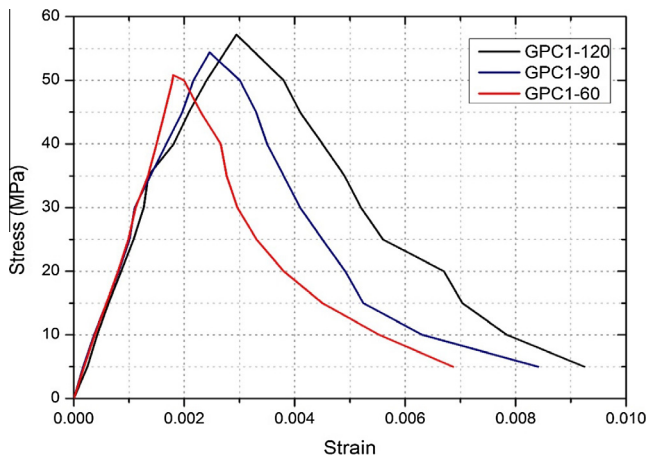| Mix	Stress (MPa)	Strain	E_c (Eq. (18)) (GPa)	E_c measured (GPa)
GPC1–60	50.8	0.0018	28.1	25.1
GPC1–90	54.4	0.0024	22.6	25.4
GPC1–120	57.2	0.0029	19.7	24.2
GPC2–60	52	0.0026	20	21.9
GPC2–90	53.6	0.0025	21.4	25.5
GPC2–120	55	0.0028	19.6	24.9
GPC3–60	46.3	0.0027	17.1	22.8
GPC3–90	49.7	0.0025	19.8	22.6
GPC3–120	52.4	0.0017	30.8	28

Fig. 12. Stress–strain curve of GPC1 at 60, 90 and 120 °C.

Fig. 13a. Predicted and test value of stress–strain relations for GPC1 at 60 °C.

Fig. 13b. Predicted and test value of stress–strain relations for GPC1 at 90 °C.

Fig. 13c. Predicted and test value of stress–strain relations for GPC1 at 120 °C.

Eqs. (15) and (16) are not used to predict the value of modulus of elasticity when compressive strength is given. Also, according to Fig. 13, the difference between measured and calculated values using Eq. (17) was approximately 10%. This number is lower than the two results from Eqs. (15) and (16), and it is acceptable to use for predicting the Young's modulus of geopolymer concrete.

5.2. Stress–strain relation in compression

In order to define the stress–strain relation of geopolymer concrete, GPC1 with curing conditions 60, 90, and 120 °C for 10 h were used. The test data is shown in Table 8 and Fig. 12.

Young's modulus values from Table 8 are calculated as follows:

$$E_c = \frac{\sigma}{\varepsilon} \ (MPa) \tag{18}$$

where
  σ: Stress (MPa)
  ε: Strain

According to Hardjito [23], the strain at the peak stress of geopolymer concrete is in the range 0.0024–0.0026. From Fig. 12, the strain of fly-ash geopolymer concrete is about 0.0018–0.0029. However, most values were within the range 0.0024–0.0026. These values are similar to those of conventional concrete. The Young's modulus value calculated from the stress–strain curve by using Eq. (17) was about 15% different from the measured Young's modulus value.

Collins et al. [24] proposed that the stress–strain relation of Portland cement concrete in compression can be predicted using the expression:
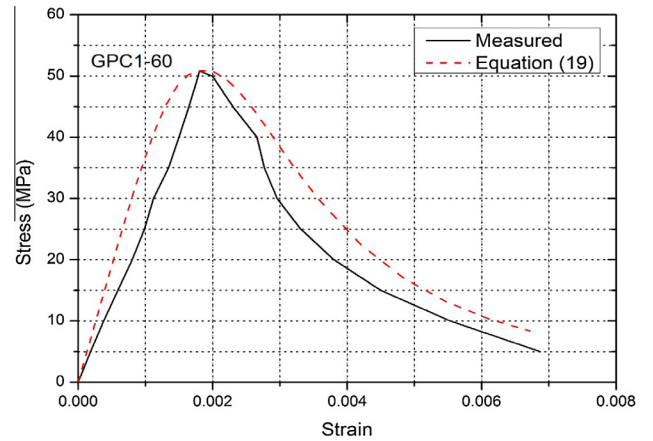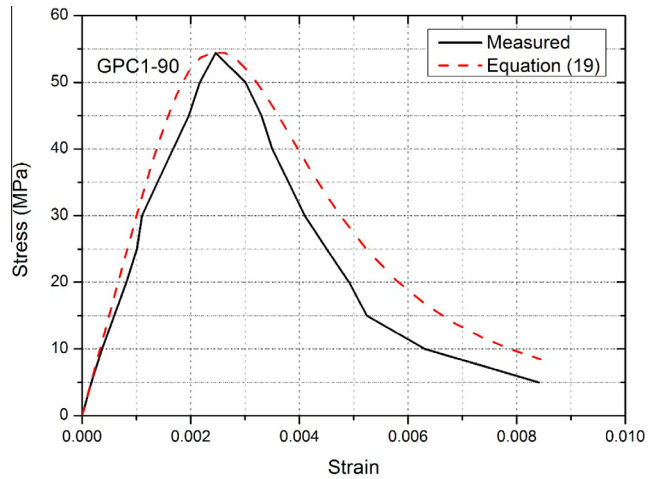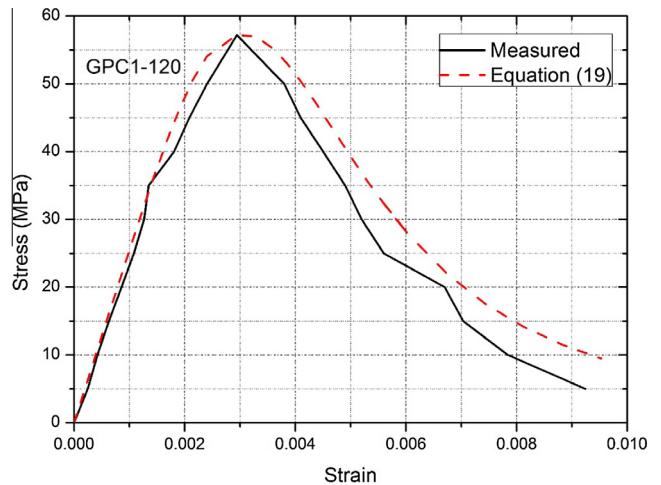
$$\sigma_c = f_{cm} \frac{\varepsilon_c}{\varepsilon_{cm}} \frac{n}{n - 1 + \left(\frac{\varepsilon_c}{\varepsilon_{cm}}\right)^{nk}} \tag{19}$$

where
  f_{cm}: peak stress

ε_{cm}: strain at peak stress
$n = 0.8 + (f_{cm}/17)$
$k = 0.67 + (f_{cm}/62)$ when $\varepsilon_c/\varepsilon_{cm} > 1$ or
$k = 1$ when $\varepsilon_c/\varepsilon_{cm} \leqslant 1$

From Figs. 13a–c, the stress–strain curves predicted by Eq. (19) are compared with the test curves given in Fig. 12. The analytical curves were calculated using the measured values f_{cm} and ε_{cm} in Eq. (19). From Figs. 13a–c, the test curves correlated well with the analytical curves. In general, Eq. (19) could be used to predict the stress–strain relation of geopolymer concrete.

5.3. Indirect tensile strength

The tensile strength of fly-ash-based geopolymer concrete was done in accordance with ASTM C496. The mixtures GPC1, GPC2, and GPC3 were used in 150 × 300 mm concrete cylinders. These specimens were tested after curing in an oven at 60, 90, or 120 °C for 4, 6, 8, and 10 h. The test results are shown in Fig. 14.

From Fig. 14, the tensile strength of geopolymer concrete is from 3 MPa to 4.5 MPa, so the tensile strength of geopolymer concrete is nearly higher than that of OPC. This can be explained by the fact that the connection between geopolymer binder and aggregate is stronger. According to Lee et al. [26], the effects of solube silicate addition were twofold. First, solube silicates were effective in reducing alkali saturation in the concrete pore. Then, they promoted greater interparticle bonding within the geopolymeric binders to the aggregates surface. As a result, denser binders formed the stronger aggregate and binder interfaces. Thus, it is more difficult to cut the link between them. The tensile strength of geopoly-

mer concrete is also effected by curing conditions. Higher curing temperature and longer curing time result in greater tensile strength.

Hardjito [23] proposed a formula to calculate the indirect tensile strength:

$$f_{ct} = 0.7\sqrt{f_{cm}} \text{ (MPa)} \tag{20}$$

Standards Australia [25] recommends using the following expression to determine the tensile strength of OPC concrete:

$$f_{ct} = 0.4\sqrt{f_{cm}} \text{ (MPa)} \tag{21}$$

Neville [19] has recommended that the relation between the tensile splitting strength and the compressive strength of Portland cement concrete be expressed as:

$$f_{ct} = 0.3(f_{cm})^{2/3} \text{ (MPa)} \tag{22}$$

where

f_{ct}: the tensile strength (MPa)
f_{cm}: the compressive strength (MPa)

According to previous researchers, the tensile splitting strength of geopolymer concrete is only a fraction of the compressive strength, as it is for Portland cement concrete.

Fig. 15 shows the relationship between compressive strength and tensile strength according to Eqs. (20)–(22), and the measurement method. The values for geopolymer concrete are higher than for OPC. And the measured values are near by the values from Eq. (20). The difference is about 10–15%.
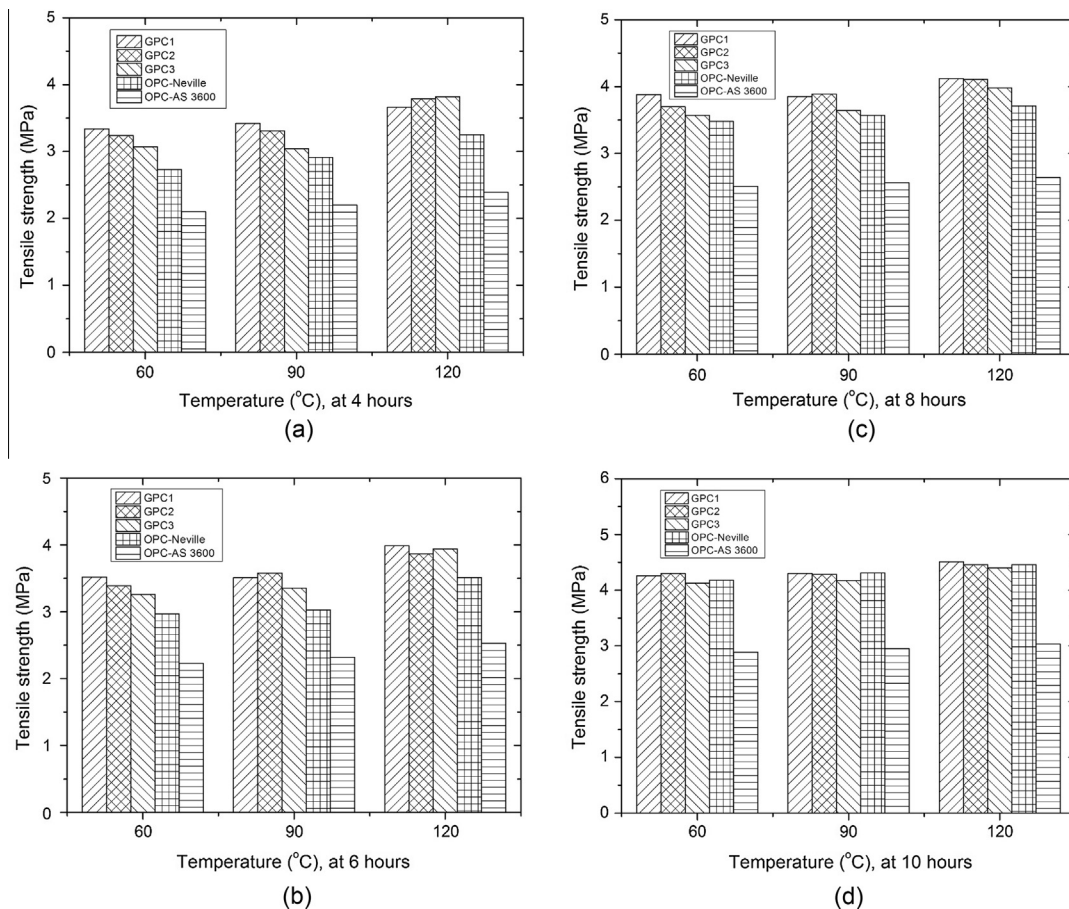

Fig. 14. Tensile strength of geopolymer concrete with change of curing time and curing temperature.
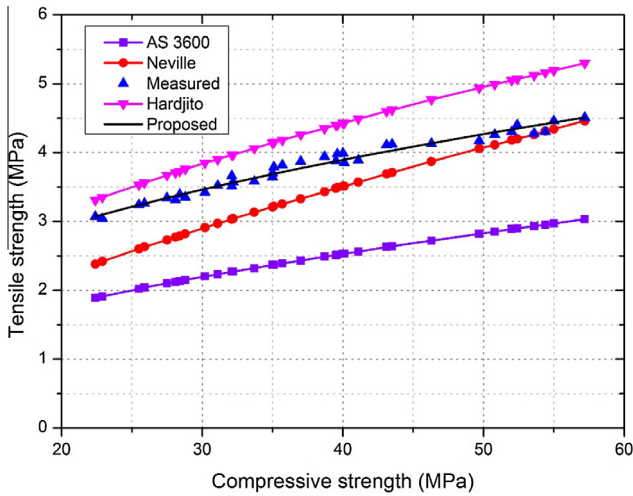
Fig. 15. Relationship between compressive strength and tensile strength.

In this paper, a new formula is proposed that uses test data from Fig. 15. This formula was used to calculate the tensile strength when the compressive strength is given:

$$f_{ct} = 0.858(f_{cm})^{0.410} \text{ (MPa)} \tag{23}$$

where

 f_{ct}: the tensile strength (MPa)
  f_{cm}: the compressive strength (MPa)

### 5.4. Flexural performance of fly ash-geopolymer concrete beam

The results shown in Fig. 16 were obtained in three different ways: theoretical analysis based on elastic theory, FE model using ABAQUS and experimental test. The theoretical load–deflection curve was determined using Eq. (10). The FE model was used to simulate the experimental beam shown in Fig. 3. From Fig. 16a–c, it can be seen that the load–deflection curve of the FEM and that from the experimental test are very similar, especially a near match for GPC1. For GPC2 and GPC3, up to the first 2 mm deflection, the FEM models are much stiffer than experimental model. However from 2 mm deflection, the deflection difference of FEM models and experimental model is gradually reduced and convergent before the model is failed. In contrast, the load–deflection curve generated by elastic theory looks different from the others. In general, the actual beam is stiffer than suggested by the theoretical analysis model.

The difference between theory and experiment might be due to several factors. First, the bond strength between concrete and the reinforcing bar is neglected in theoretical analysis; however, this would be not true for the actual beam model. Second, the elastic theory is designed for normal concrete. For geopolymer concrete, there is a need to add some modifications to suit this new material.

The data in Fig. 16 also shows fair agreement between ABAQUS and experimental test results. The reason is that the FE model was intended to be an exact replicate of the actual beam, but there are still differences. When the actual beam works during the four-point bending test, friction forces appear at the supports and loading rollers. However, it is difficult to determine this kind of force under real conditions. Thus, the friction forces are neglected when the model is simulated by ABAQUS. Instead of the frictional behavior between supports or loading rollers and the beam, the property "Tie" is given when the relationship between the beam model, and the supports and loading rollers, is described in ABAQUS. Moreover, the re-bars are given the property "Embedded" (in Con-
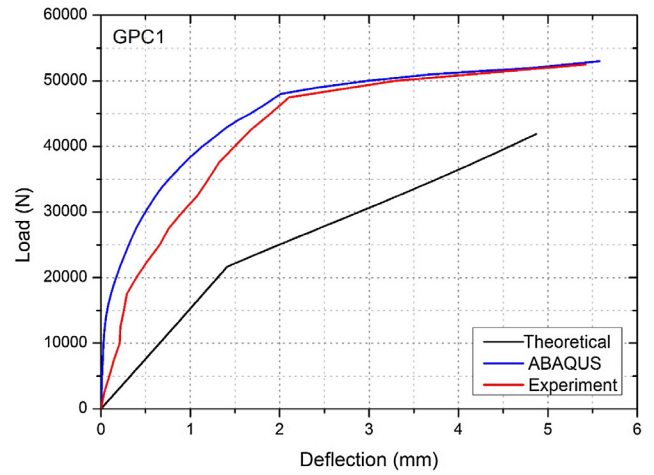
(a) GPC1
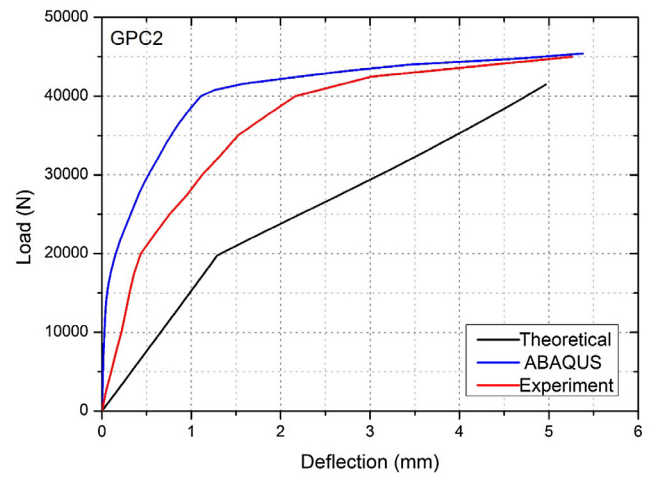
(b) GPC2
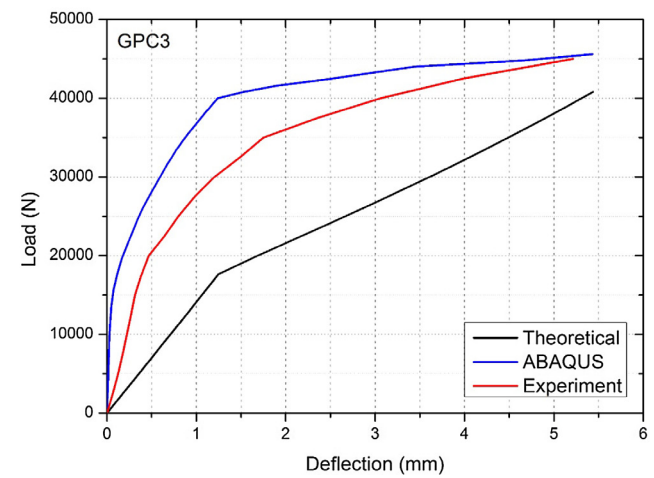
(c) GPC3

Fig. 16. Load deflection curve of the geopolymer concrete beam.

straints) and the simulation includes composite action between concrete and steel. However, in the actual beam, slip occurs, so this assumption would not be true. These factors affect the final result, and are the main reasons for inconsistency in the simulated and experimental results.
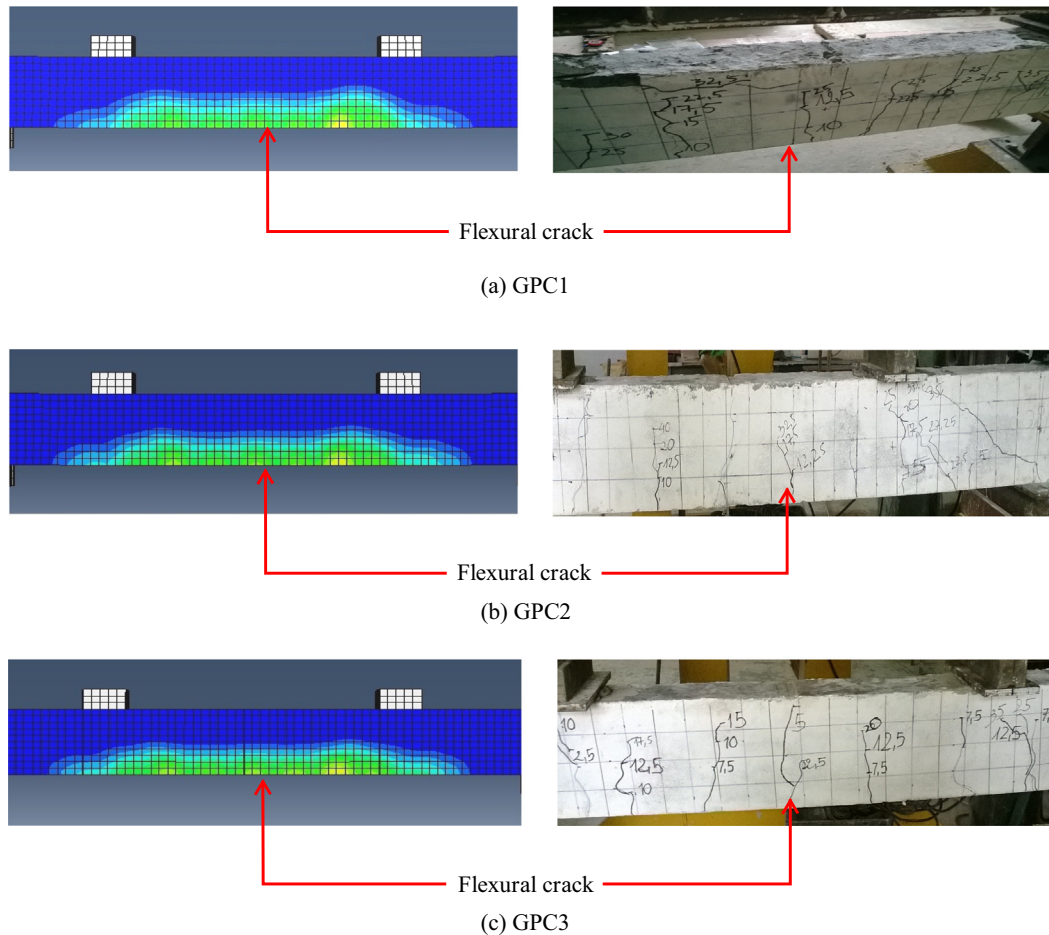
(a) GPC1

(b) GPC2

(c) GPC3

Fig. 17. Crack patterns of experimental beams.

For each applied load step, a crack pattern was created using ABAQUS program. A comparison of the concrete patterns from the numerical results, with those obtained by experimental test, is shown in Fig. 17. In general, flexural cracks occur early at mid-span. When the loads increase, vertical flexural cracks spread horizontally from the mid span to the support. At higher loads, diagonal cracks appear. Increasing the load even more produces additional diagonal and flexural cracks. There is good agreement between the crack patterns of fly-ash-based geopolymer concrete generated by FE analysis using ABAQUS, and those in the experimental data.

6. Conclusions

In this research, the mechanical properties of heat-cured low-calcium fly-ash-based geopolymer concrete and its behavior were investigated. In order to evaluate these properties, experiments were conducted using 150×300 mm cylindrical specimens, and $100\ (b) \times 200\ (h) \times 2000$ mm (L) beam models. The important points and conclusions from this investigation are summarized below.

1. The measured values of the modulus elasticity of heat-cured low-calcium fly-ash-based geopolymer concrete, with compressive strength in the range 45–58 MPa, were different from those of conventional concrete. These measured values are lower than the values calculated using the current standards AS 3600 and ACI 363. However, these measured values are similar to the values calculated using the formula proposed by Hardjito. More-

over, the modulus elasticity of geopolymer concrete is affected by its microstructure based on speciation caused by the alkali silicate activating solution. This is different from normal concrete, for which Young's modulus depends on the properties of the aggregate.

2. The Poisson's ratio of fly-ash-based geopolymer concrete with compressive strength in the range of 45–58 MPa, is from 0.16 to 0.21. These values are similar to the values of conventional concrete. The stress–strain relations of heat-cured fly-ash-based geopolymer concrete in compression well match the formulation designed for Portland cement concrete.

3. The measured indirect tensile strength of fly-ash geopolymer concrete is greater than the values calculated using an expression designed for Portland cement concrete. However, as with Portland cement, this value is also predicted by using a proposed formula as a fraction of the compressive strength.

4. The behavior of heat-cured low-calcium fly-ash-based geopolymer concrete is good agreement in the FE simulation using ABAQUS. However, its behavior is quite different from the results provided by elastic theory designed for OPC. The actual geopolymer beam is stiffer than the theoretical analysis model. The measured deflections of beam and the predicted deflection using ABAQUS agree quite well.

Acknowledgement

References

[1] R. McCaffrey, Climate change and the cement industry, Global Cem. Lime Mag. (2002) 15–19.

[2] J. Davidovits, Global warming impact on the cement and aggregates industries, World Resour. Rev. 46 (1999) 263–278.

[3] J. Davidovits, Synthesis of new high temperature geopolymers for reinforced plastics/composites, SPE PACTEC, Soc. Plast. Eng. 79 (1979) 151–154.

[4] J. Davidovits, Ancient and modern concretes: what is the real difference, Concr. Int. 12 (1987) 23–25.

[5] J. Davidovits, Geopolymer Chemistry and Applications, third ed., Institut Geopolymer, France, 2011.

[6] P. Duxson, Effect of alkali cations on aluminum incorporation in geopolymeric gels, Ind. Eng. Chem. Res. 44 (2005) 832–839.

[7] N. Ganesan, R. Abraham, R.S. Deepa, D. Sasi, Stress–strain behavior of confined geopolymer concrete, Constr. Build. Mater. 73 (2014) 236–331.

[8] N.J. Brooke, L.M. Keyte, W. South, L.M. Megget, J.M. Ingham, Seismic performance of 'green concrete' interior beam-column joints, in: Proceeding of Australian Structural Engineering Conference (ASEC) 2005, Newcastle.

[9] K. Uma, R. Anuradha, R. Venkatasubramani, Experimental investigation and analytical modeling of reinforced geopolymer concrete beam, Int. J. Civ. Struct. Eng. (2012) 3.

[10] M.D.J. Sumajouw, B.V. Rangan, Low calcium fly ash-based geopolymer concrete: reinforced beams and columns. Research report GC-3 2006, Faculty of Engineering, Curtin University of Technology, Perth, Australia.

[11] ASTM C 39/C 39M, Standard Test Method for Compressive Strength of Cylindrical Concrete Specimen.

[12] ASTM C469, Standard Test Method for Static Modulus of Elasticity and Poison's Ratio of Concrete in Compression.

[13] ASTM C496, Standard Test Method for Splitting Tensile Strength of Concrete.

[14] F. Mujika, On the difference between flexural moduli obtained by three-point and four-point bending tests, Polym. Test 214–220 (2006).

[15] ACI Committee 318. Building Code Requirements for Reinforced Concrete, American Concrete Institute, USA.

[16] S. Hamid, Evaluation of reinforce concrete beam behavior using finite element analysis by ABAQUS, Sci. Res. Essays 7 (2012) 2002–2009.

[17] K. Lee, J. Han, Fatigue behavior of composite beams with pyramidal shear connectors under repeated loading, KSCE J. Civ. Eng. 2 (1998) 119–128.

[18] H.T. Hu, J.I. Liang, Ultimate analysis of BWR Mark III reinforced concrete containment subjected to internal pressure, Nucl. Eng. Des. 195 (2000) 1–11.

[19] A.M. Neville, Properties of Concrete, fourth ed., Wiley, New York, 2000.

[20] P. Duxson, J.L. Provis, G.C. Lukey, S.W. Mallicoat, W.M. Kriven, J.S.J. van Deventer, Understanding the relationship between geopolymer composition, microstructure and mechanical properties, Coll. Surf. A. Physiochem. Eng. Asp. 269 (2005) 47–58.

[21] ACI Committee 363, State of the Art Report on High-Strength Concrete, American Concrete Institute, Detroit. USA, 1992.

[22] Standards Australia AS 3600. Methods of testing concrete. Method 17: Determination of the static chord modulus of elasticity and Poisson's ratio of concrete specimens, 2005.

[23] D. Hardjito, B.V. Rangan, Development and properties of low-calcium fly ash based geopolymer concrete. Research report GC-1 2005, Faculty of Engineering, Curtin University of Technology, Perth, Australia.

[24] M.P. Collins, D. Mitchell, J.G. MacGregor, Structural design considerations for high strength concrete, ACI Concr. Int. 15 (1993) 27–34.

[25] Standards Australia 2001. Concrete Structures, AS3600-2001.

[26] W.K.W. Lee, J.S.J.V. Deventer, The interface between natural siliceous aggregates and geopolymers, Cem. Concr. Res. 34 (2004) 195–206.